

K-MaT: Knowledge-Anchored Manifold Transport for Cross-Modal Prompt Learning in Medical Imaging

Jiajun Zeng¹ and Shadi Albarqouni¹[✉]

University of Bonn, University Hospital Bonn, Clinic for Diagnostic and
Interventional Radiology, 53127 Bonn, Germany
{Zeng.Jiajun, Shadi.Albarqouni}@ukbonn.de

Abstract. Large-scale biomedical vision-language models (VLMs) adapted on high-end imaging (e.g., CT) often fail to transfer to frontline low-end modalities (e.g., radiography), collapsing into modality-specific shortcuts. We propose K-MaT (Knowledge-Anchored Manifold Transport), a prompt-learning framework that transfers decision structures to low-end modalities without requiring low-end training images. K-MaT factorizes prompts, anchors them to clinical text descriptions, and aligns the low-end prompt manifold to the visually-grounded high-end space using Fused Gromov-Wasserstein optimal transport. We evaluate K-MaT on four cross-modal benchmarks, including dermoscopy, mammography to ultrasound, and CT to chest X-ray. K-MaT achieves state-of-the-art results, improving the average harmonic mean of accuracy to 44.1% (from BiomedCoOp’s 42.0%) and macro-F1 to 36.2%. Notably, on the challenging breast imaging task, it mitigates the catastrophic forgetting seen in standard methods like CoOp (which drops to 27.0% accuracy on the low-end), preserving robust performance across modalities. Aligning prompt manifolds via optimal transport provides a highly effective route for the zero-shot cross-modal deployment of medical VLMs.

Keywords: Vision Language Models · Prompt Tuning · Optimal Transport · Cross-modal transfer

1 Introduction

Deep learning models for medical imaging often degrade under distribution shifts, particularly during cross-modal transfer where distinct acquisition physics encourage modality-specific shortcuts [7, 13, 3]. For instance, models trained on high-end screening modalities (e.g., MRI, CT) rarely generalize reliably to accessible, frontline modalities (e.g., X-ray and Ultrasound), despite targeting identical underlying pathologies.

Vision-language models (VLMs) and prompt learning offer efficient adaptation paradigms without full finetuning [10, 15, 17]. While BiomedCLIP exhibits

[✉] Corresponding author.

high generalization, it struggles with specific tasks. CoOp and its variants [17, 12] attempt to optimize unified prompts to help models generalize across seen and unseen classes; however, these prompts are prone to overfit to seen classes and domains. Furthermore, while BiomedCoOp [5] improves low-shot biomedical transfer using Large Language Model (LLM)-generated visual descriptions and knowledge distillation from zero-shot BiomedCLIP, it still suffers from similar problems. In cross-modal settings, we observe that learnable prompts optimized exclusively on high-end modalities suffer from *catastrophic knowledge forgetting*—they collapse into modality-specific statistics and fail to preserve the essential general textual knowledge required for shared diagnostic semantics [6].

To address this, we study asymmetric cross-modal knowledge transfer and ask whether diagnostic semantics learned from high-end visual data can be reliably transferred to low-end modalities in a strict zero-shot regime. We build on the BiomedCLIP [15] backbone and propose **K-MaT (Knowledge-Anchored Manifold Transport)**, a structure-preserving factorized prompt learning framework. Our core contributions are: (i) We introduce a strict zero-shot asymmetric transfer strategy relying solely on high-end visual data and LLM-generated clinical descriptions, eliminating the need for low-end visual training data. (ii) We mitigate catastrophic forgetting via a novel *space anchoring* constraint, treating LLM-generated textual prototypes as semantic anchors to prevent deviation from clinically meaningful semantics. (iii) We propose a cross-modal manifold alignment objective using Fused Gromov-Wasserstein (FGW) optimal transport [11], enforcing the learned low-end prompt manifold to strictly mirror the visually grounded relational structure of the high-end manifold. (iv) Validated on four cross-modal dataset pairs, our approach successfully prevents the decision boundary from collapsing into modality-specific shortcuts, achieving competitive zero-shot generalization against baselines that require target domain data.

2 Proposed Method

In this section, we detail our proposed K-MaT prompt learning framework for asymmetric cross-modal transfer, as depicted in Fig. 1. Here, comprehensive screening uses a high-end source modality \mathcal{X}_H , while frontline assessments rely on a low-end target modality \mathcal{X}_L . We aim for High-to-Low generalization by performing few-shot learning on \mathcal{X}_H and zero-shot inference on \mathcal{X}_L , entirely bypassing low-end visual data.

Backbone Model and Prompt Parameterization. Following the prompt tuning paradigm, we build upon a frozen biomedical VLM (BiomedCLIP [15]) containing a visual encoder $\phi(\cdot)$ and a textual encoder $\theta(\cdot)$. We freeze the pre-trained visual and textual encoders and adapt the model via learnable context vectors. For a downstream task consisting of N_c categories, we introduce learnable context vectors to generate task-related textual embeddings. For the i -th class token \mathbf{c}_i and modality $m \in \{H, L\}$, we define a factorized learnable prompt:

$$\mathbf{t}_{i,m} = [\mathbf{v}_{i,m}^1, \mathbf{v}_{i,m}^2, \mathbf{v}_{i,m}^3, \mathbf{v}_{i,m}^4, \mathbf{c}_i]$$

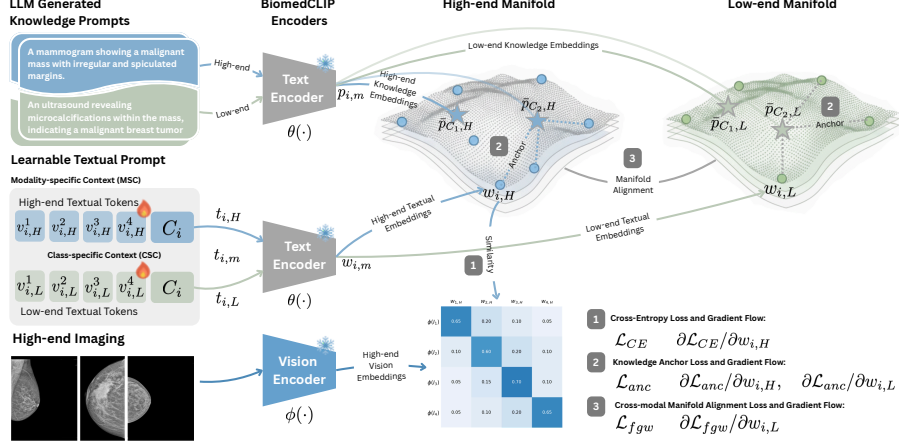


Fig. 1. Overall architecture of the proposed K-MaT framework. During training, high-end textual prompts are optimized using high-end imaging data (\mathcal{L}_{ce}), while prompts from both modalities are anchored to LLM-generated clinical descriptions (\mathcal{L}_{anc}). The low-end prompt manifold is strictly aligned to the visually grounded high-end space via \mathcal{L}_{fgw} . During inference, the frozen visual encoder extracts features from unseen low-end images, and predictions are computed via visual-textual similarity with the learned low-end embeddings, bypassing low-end visual training entirely.

where $\mathbf{v}_{i,m}^k$ denote the modality-specific and class-specific learnable context tokens. The specific textual embedding $w_{i,m}$ is obtained by feeding the learnable prompt $\mathbf{t}_{i,m}$ into the textual encoder $\theta(\cdot)$, i.e., $w_{i,m} = \theta(\mathbf{t}_{i,m})$.

High-end Supervised Training. During training, we utilize labeled images exclusively from the high-end modality \mathcal{X}_H . Given an image $I_H \in \mathcal{X}_H$ along with its label y , the visual embedding is extracted with the visual encoder: $x_H = \phi(I_H)$. We optimize the high-end learnable prompts $\mathbf{t}_{i,H}$ by minimizing the standard cross-entropy loss:

$$\mathcal{L}_{ce} = -\frac{1}{N} \sum_{I_H \in \mathcal{X}_H} \log p(y|x_H, w_{i,H}) = -\frac{1}{N} \sum_{I_H \in \mathcal{X}_H} \log \frac{\exp(d(x_H, w_{y,H})/\tau)}{\sum_{i=1}^{N_c} \exp(d(x_H, w_{i,H})/\tau)}$$

where τ is a predefined temperature parameter, N is the number of images, and $d(\cdot)$ is the cosine similarity between the visual embedding x_H and the textual embeddings $w_{i,H}$. This objective updates the high-end learnable prompts, explicitly injecting high-end visual knowledge into the textual embedding space.

Space Anchoring to Modality-Specific Lexical Prompts. While learnable prompts capture discriminative task-specific knowledge, they risk collapsing into modality-specific statistics and forgetting the essential general textual knowledge. To alleviate this, we define general textual knowledge using a fixed ensemble of visual descriptions. To reduce the reliance on manual domain expertise while providing precise prior knowledge, we employ an LLM to automatically generate these descriptions. Let $p_{i,m}^j$ denote the j -th LLM-generated

visual description for the i -th class under modality m , where $j \in \{1, \dots, N_p\}$ and N_p is the number of descriptions per class. We feed these generated descriptions into the textual encoder to generate the general textual prototype embedding, $\bar{p}_{i,m} = \frac{1}{N_p} \sum_{j=1}^{N_p} \theta(p_{i,m}^j)$, which remains fixed during training. To ensure the learnable specific textual knowledge acts as a semantic anchor and does not deviate from clinically meaningful semantics, we introduce a space anchoring constraint that minimizes the discrepancy (Euclidean distance) between the general textual prototypes and the learnable specific textual embeddings:

$$\mathcal{L}_{anc} = \frac{1}{2N_c} \sum_{i=1}^{N_c} \sum_{m \in \{H,L\}} \|w_{i,m} - \bar{p}_{i,m}\|_2^2$$

As the class and modality tokens are fixed, gradients from \mathcal{L}_{anc} solely update the shared and modality-specific learnable tokens.

Cross-modal Manifold Alignment via FGW. To further prevent the decision boundary from collapsing into high-end specific statistics, we propose a novel alignment objective based on the FGW optimal transport [11]. FGW acts as a structural regularizer, enforcing the learned low-end prompt manifold to strictly mirror the relational structure of the high-end prompt manifold anchored by clinical text knowledge. To explicitly focus this alignment on modality-specific structure, we treat the high-end textual embeddings as a fixed reference manifold. Let $\tilde{w}_{i,H}$ and $\tilde{w}_{j,L}$ denote the textual embeddings for the i -th class in the high-end modality and the j -th class in the low-end modality, where $i, j \in \{1, \dots, N_c\}$. We first compute the intra-modal structural distance matrices $D^H, D^L \in \mathbb{R}^{N_c \times N_c}$ with elements, $D_{ik}^H = \|\tilde{w}_{i,H} - \tilde{w}_{k,H}\|_2$, $D_{jl}^L = \|\tilde{w}_{j,L} - \tilde{w}_{l,L}\|_2$, where indices i, k iterate over the high-end classes and j, l iterate over the low-end classes. Alongside this, we compute the cross-modal feature cost matrix $M \in \mathbb{R}^{N_c \times N_c}$ with elements $M_{ij} = \|\tilde{w}_{i,H} - \tilde{w}_{j,L}\|_2^2$. FGW seeks an optimal coupling matrix $\Gamma \in \mathbb{R}_+^{N_c \times N_c}$ to jointly align the feature representations and the relational geometric structure. The corresponding constraint is formulated as:

$$\mathcal{L}_{fgw} = (1 - \alpha) \sum_{i,j=1}^{N_c} M_{ij} \Gamma_{ij} + \alpha \sum_{i,j,k,l=1}^{N_c} |D_{ik}^H - D_{jl}^L|^2 \Gamma_{ij} \Gamma_{kl}$$

where $\alpha \in [0, 1]$ is the trade-off parameter balancing the Wasserstein feature alignment and the Gromov-Wasserstein structural alignment. For FGW, we detach high-end embeddings and backpropagate only into low-end prompt embeddings. Intuitively, \mathcal{L}_{FGW} ensures the low-end prompt manifold preserves the shared diagnostic semantics anchored by the fixed high-end space, entirely by-passing the need for low-end visual training data.

Overall Objective and Inference. The final objective combines cross-entropy loss with knowledge anchoring and manifold alignment constraints:

$$\mathcal{L} = \mathcal{L}_{ce} + \lambda_{anc} \mathcal{L}_{anc} + \lambda_{fgw} \mathcal{L}_{fgw}$$

where λ_{anc} and λ_{fgw} balance the effect of the respective regularization terms. During inference, the learned low-end embeddings $w_{i,L}$ are used to classify unseen images $I_L \in \mathcal{X}_L$ by computing the visual-textual similarity $p(y|x_L, w_{i,L})$, $x_L = \phi(I_L)$ with frozen encoders. During this phase, all visual and textual backbone parameters remain strictly frozen.

3 Experiments and Results

3.1 Experimental Settings

Datasets and Tasks. We evaluate our proposed K-MaT on 4 diverse cross-modal medical imaging pairs covering various clinical tasks. Specifically, the evaluation encompasses: (1) skin lesion classification transferring from Dermoscopy to Clinical Images (DERM7PT) [4]; (2) skin lesion classification transferring from Dermoscopy to 15cm Clinical Images (MRA-MIDAS) [2]; (3) breast lesion classification from Mammography [8] to Ultrasound [1]; and (4) COVID-19 pneumonia classification from CT [14] to Chest X-ray [9]. We also use GPT-5 to generate $N_p = 50$ visual descriptions for each class and modality. Table 1 summarizes the dataset statistics and domain characteristics..

Implementation Details. We adopt the pre-trained BiomedCLIP as our frozen backbone. For prompt tuning, we randomly initialize a learnable context of length 4. To ensure effective transfer and mitigate interference between modality classes, we introduce Class-Specific Context (CSC) and Modality-Specific Context (MSC), learning distinct prompts for each class across different modalities.

The model is optimized for 50 epochs (batch size 4) using the SGD optimizer with a 0.0025 base learning rate, a cosine annealing scheduler, and a 1-epoch warmup. To compute the FGW optimal coupling Γ , we use the Sinkhorn-Knopp algorithm [11] (temperature 0.1, max 100 iterations) and set the trade-off α to 0.1. All experiments use a 16-shot setting per class, with results averaged over 3 random seeds. Hyperparameters (λ_{anc} , λ_{fgw}) are tuned exclusively on the high-end validation set, leaving low-end images strictly for test-time evaluation. We run all experiments on a single NVIDIA A100 (80GB) GPU.

3.2 Experiments on Cross-modal Generalization

We compare our proposed K-MaT with BiomedCLIP and the state-of-the-art (SOTA) prompt tuning methods equipped with BiomedCLIP backbone, including CoOp [17], CoCoOp [16], KgCoOp [12], and BiomedCoOp [5]. Table 2 details the cross-modal generalization performance in terms of Accuracy and Macro-F1 scores, respectively. Across the four diverse medical image pairs, K-MaT consistently outperforms all competitive baselines, achieving the highest average Harmonic Mean (H) of 44.1% for Accuracy and 36.2% for F1 score. H is a critical evaluation metric in our asymmetric setting, as it penalizes extreme performance disparities and accurately reflects the model’s ability to retain knowledge in the source high-end modality while effectively generalizing diagnostic semantics to the unseen low-end target modality.

Table 1. Dataset statistics for the five cross-modal tasks.

Task	Type	Dataset	Modality	Classes	Train	Val	Test
Skin I	High-end	MRA-MIDAS [2]	Dermoscopy	6	513	91	135
	Low-end	MRA-MIDAS [2]	Clinical	6	501	89	132
Skin II	High-end	Derm7pt [4]	Dermoscopy	5	413	203	395
	Low-end	Derm7pt [4]	Clinical	5	413	203	395
Chest	High-end	CC-CCII [14]	CT	3	10670	3538	1678
	Low-end	ChestXray [9]	X-Ray	3	4595	923	914
Breast	High-end	DMID [8]	Mammography	3	356	76	78
	Low-end	BUSI [1]	Ultrasound	3	389	155	236

Traditional prompt learning algorithms, such as CoOp and CoCoOp, demonstrate substantial improvements on the high-end source modalities but suffer from severe catastrophic forgetting when evaluated on the low-end target modalities. For instance, in the breast dataset task (transferring from Mammography to Ultrasound), CoOp achieves a high-end accuracy of 75.2% but plummets to 27.0% on the Low-end target. Similarly, CoCoOp yields 65.0% on the High-end but only 28.2% on the Low-end. These methods tend to overfit to the distinct appearance statistics of the source domain, adopting modality-specific shortcuts rather than shared clinical semantics. K-MaT directly addresses this vulnerability; by preserving structural relationships, it prevents the decision boundary from collapsing, boosting the Low-end target accuracy to 38.4% on the Breast dataset and achieving a leading H of 50.3%.

Even when compared to BiomedCoOp, a robust recent baseline tailored specifically for biomedical VLMs, K-MaT exhibits superior generalization. Across all four benchmarks, K-MaT surpasses BiomedCoOp by a 2.1% margin in average H Accuracy (44.1% vs. 42.0%) and a 1.2% margin in average H F1 (36.2% vs. 35.0%). This demonstrates that while integrating general biomedical knowledge is beneficial, it is insufficient on its own to navigate severe cross-modal domain shifts. By explicitly aligning the relational geometry of the prompt manifold through optimal transport, K-MaT effectively distills shared clinical knowledge, successfully achieving competitive zero-shot generalization.

3.3 Ablation Study

To evaluate the contribution of each component, we conduct an ablation study to assess the impact of our prompt context designs (CSC and MSC), the space-anchoring loss \mathcal{L}_{anc} , and the FGW alignment loss \mathcal{L}_{fgw} . Table 3 presents these architectural variations across High-end, Low-end, and H metrics.

Effectiveness of Context Modularization. The baseline configuration (optimizing solely with cross-entropy \mathcal{L}_{ce}) exhibits restricted generalization. It heavily biases predictions toward the high-end, confirming that unconstrained learnable prompts risk collapsing into modality-specific shortcuts. Rows 2 and 3 in

Table 2. Cross-modal generalization performance on 4 medical image pairs with ACC and macro-F1 shown together. Each entry is reported as average ACC (F1) over 3 seeds. Hi: High-End (source), Lo: Low-End (target), H: Harmonic Mean. Best ACC/F1 results are highlighted in **bold**/underline respectively.

Dataset	BiomedCLIP	CoOp	KgCoOp	CoCoOp	BiomedCoOp	K-MaT
Skin I	Hi	34.6 (24.2)	55.5 (<u>42.3</u>)	56.6 (41.6)	44.6 (32.0)	58.3 (39.3) <u>56.8</u> (43.1)
	Lo	31.7 (21.0)	40.8 (27.1)	40.5 (<u>28.5</u>)	29.8 (24.2)	<u>42.2</u> (29.1) 46.4 (27.4)
	H	37.9 (22.9)	47.0 (33.0)	47.2 (33.9)	35.7 (27.5)	<u>49.0</u> (33.4) 50.9 (33.3)
Skin II	Hi	32.6 (26.9)	34.8 (32.1)	34.6 (32.7)	40.7 (36.7)	<u>35.6</u> (31.8) 34.8 (32.8)
	Lo	17.4 (13.6)	<u>28.5</u> (<u>26.4</u>)	<u>28.5</u> (27.3)	18.4 (18.0)	27.0 (24.6) 31.6 (25.0)
	H	22.7 (18.1)	<u>31.4</u> (<u>29.0</u>)	31.3 (29.8)	25.4 (24.2)	30.7 (27.7) 33.1 (28.3)
Chest	Hi	34.0 (24.6)	<u>52.0</u> (<u>47.8</u>)	47.1 (42.3)	37.4 (36.3)	43.4 (40.9) 54.5 (50.8)
	Lo	29.9 (<u>32.1</u>)	26.4 (21.8)	26.1 (<u>22.7</u>)	54.5 (35.6)	38.7 (29.2) <u>40.6</u> (31.1)
	H	31.8 (27.9)	35.0 (30.0)	33.6 (29.5)	44.4 (35.9)	40.9 (34.0) <u>42.3</u> (<u>35.4</u>)
Breast	Hi	24.4 (19.9)	75.2 (72.8)	70.5 (66.6)	65.0 (59.5)	69.2 (65.0) <u>73.1</u> (<u>70.7</u>)
	Lo	57.2 (45.2)	27.0 (19.0)	28.0 (16.9)	28.3 (26.6)	36.0 (34.1) <u>38.4</u> (<u>36.3</u>)
	H	34.2 (27.7)	39.7 (30.2)	40.1 (27.0)	39.4 (36.8)	<u>47.4</u> (<u>44.8</u>) 50.3 (47.9)
Avg.	Hi	34.6 (24.2)	<u>54.4</u> (<u>48.7</u>)	52.2 (45.8)	46.9 (41.1)	51.6 (44.2) 54.8 (49.3)
	Lo	34.0 (28.0)	30.7 (23.6)	30.8 (23.9)	32.7 (26.1)	<u>36.0</u> (<u>29.2</u>) 39.3 (29.9)
	H	31.7 (24.1)	38.3 (30.5)	38.0 (30.0)	36.2 (31.1)	<u>42.0</u> (<u>35.0</u>) 44.1 (36.2)

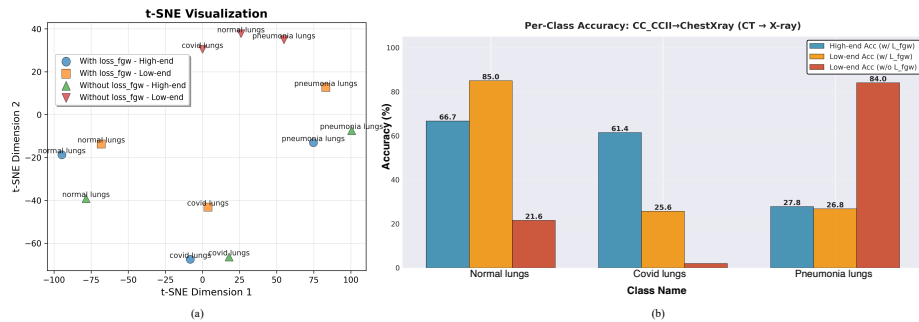
Tab. 3 show that the combination of CSC and MSC can mitigate interference between modality classes and ensure effective cross-modal transfer with the relative improvement from -12.03% to -5.31% of Acc. The row 6 and 7 indicate that MSC could improve cross-modal performance (36.67% Acc) but affect the Acc of high-end. While CSC slightly enhances high-end performance, it disrupts the equilibrium between high-end and low-end modalities.

Effectiveness of Semantic Anchoring and Manifold Alignment. Introducing \mathcal{L}_{anc} provides a critical regularizing effect by anchoring learnable embeddings to LLM-generated textual prototypes, preventing semantic divergence and improving the H accuracy to 41.94% (row 5). Building on this, \mathcal{L}_{fgw} acts as a powerful structural regularizer. While \mathcal{L}_{anc} maintains semantic fidelity, \mathcal{L}_{fgw} explicitly enforces the low-end prompt manifold to mirror the relational geometry of the high-end space. As shown in Table 3, the complete K-MaT framework—combining CSC, MSC, \mathcal{L}_{anc} , and \mathcal{L}_{fgw} —achieves the highest overall performance. This full configuration yields a significant 13.75% relative improvement in H F1 and a 10.10% boost in H accuracy over the baseline (Row 8).

Effectiveness of FGW. To further investigate the role of \mathcal{L}_{fgw} , we perform a t-SNE visualization and a breakdown analysis on the chest cross-modal generalization task. Specifically, we compare variants of K-MaT excluding \mathcal{L}_{anc} with and without the addition of \mathcal{L}_{fgw} . As observed in Fig. 2(a), high-end text embeddings $w_{i,H}$ act as anchors due to reliable supervision from labels and visual signals (blue circles and green triangles). By incorporating \mathcal{L}_{fgw} , the low-end

Table 3. Complete ablation study results across all dataset pairs. Relative improvement (%) is computed on the Harmonic Mean ACC/F1 with respect to the first row.

CSC	MSC	\mathcal{L}_{anc}	\mathcal{L}_{fgw}	High-end		Low-end		Harmonic Mean		Rel. Impr. (%)	
				ACC	F1	ACC	F1	ACC	F1	ACC	F1
				53.36	47.53	35.27	25.72	40.08	31.85	0.00	0.00
✓				54.02	48.49	27.55	22.71	35.26	30.03	-12.03	-5.71
✓	✓			54.69	49.17	34.73	18.68	37.95	25.83	-5.31	-18.90
✓	✓	✓		54.80	49.34	30.95	20.73	35.15	27.82	-12.30	-12.65
✓	✓		✓	54.69	49.17	36.99	26.58	41.94	32.65	4.64	2.51
✓		✓	✓	50.68	44.70	30.07	24.24	36.67	30.67	-8.51	-3.70
✓		✓	✓	53.56	48.07	28.18	22.94	35.92	30.29	-10.38	-4.90
✓	✓	✓	✓	54.80	49.34	39.25	29.92	44.13	36.23	10.10	13.75

**Fig. 2.** (a). Visualization of textual embeddings w/ and w/o \mathcal{L}_{fgw} on the Chest cross-modal generalization task. (b). The breakdown of Accuracy for each class.

embeddings $w_{i,L}$ tend to preserve the relative structure of their high-end counterparts (yellow squares). In contrast, text embeddings learned without \mathcal{L}_{fgw} fail to generate discriminative representations (red triangles). This is further confirmed by the breakdown analysis in Fig. 2(b): \mathcal{L}_{fgw} prevents the model from collapsing into a single class, improving average performance on the low-end modality through structural transport from the high-end space.

4 Conclusion

We proposed K-MaT, a zero-shot prompt learning framework for asymmetric cross-modal transfer in medical imaging. By factorizing prompts, anchoring them to LLM-generated clinical text, and aligning manifolds via FGW optimal transport, K-MaT effectively mitigates catastrophic forgetting and achieves SOTA harmonic mean performance across four benchmarks. Despite these promising results, our framework exhibits certain limitations. First, its absolute performance on low-end modalities shows limited improvement over the zero-shot Biomed-

CLIP baseline. Second, the framework is sensitive to dataset characteristics; severe visual discrepancies between modalities can create visual-textual gaps that purely text-anchored alignment cannot fully bridge. Future work will explore incorporating more reliable visual signals to enhance the stability and low-end transfer capabilities of the framework.

Acknowledgments. J. Zeng is funded by the China Scholarship Council (CSC) program (grant No. 202508440222).

Disclosure of Interests. The authors have no competing interests.

References

1. Al-Dhabyani, W., Gomaa, M., Khaled, H., Fahmy, A.: Dataset of breast ultrasound images. *Data in brief* **28**, 104863 (2020)
2. Chiou, A.S., Omiye, J.A., Gui, H., Swetter, S.M., Ko, J.M., Gastman, B., Arbesman, J., Cai, Z.R., Gevaert, O., Sadée, C., et al.: Multimodal image dataset for ai-based skin cancer (midas) benchmarking. *NEJM AI* **2**(6), AIdbp2400732 (2025)
3. Gulrajani, I., Lopez-Paz, D.: In search of lost domain generalization. arXiv preprint arXiv:2007.01434 (2020)
4. Kawahara, J., Daneshvar, S., Argenziano, G., Hamarneh, G.: Seven-point checklist and skin lesion classification using multitask multimodal neural nets. *IEEE Journal of Biomedical and Health Informatics* **23**(2), 538–546 (mar 2019). <https://doi.org/10.1109/JBHI.2018.2824327>
5. Koleilat, T., Asgariandehkordi, H., Rivaz, H., Xiao, Y.: Biomedcoop: Learning to prompt for biomedical vision-language models. In: *Proceedings of the Computer Vision and Pattern Recognition Conference*. pp. 14766–14776 (2025)
6. Liu, W., Zhu, F., Wei, L., Tian, Q.: C-clip: Multimodal continual learning for vision-language model. In: *The Thirteenth International Conference on Learning Representations* (2025)
7. Matta, S., Lamard, M., Zhang, P., Le Guilcher, A., Borderie, L., Cochener, B., Quéllec, G.: A systematic review of generalization research in medical image classification. *Computers in biology and medicine* **183**, 109256 (2024)
8. Oza, P., Oza, U., Oza, R., Sharma, P., Patel, S., Kumar, P., Gohel, B.: Digital mammography dataset for breast cancer diagnosis research (dmid) with breast mass segmentation analysis. *Biomedical Engineering Letters* **14**(2), 317–330 (2024)
9. Patel, P.: Chest X-ray (Covid-19 & pneumonia). <https://www.kaggle.com/datasets/prashant268/chest-xray-covid19-pneumonia> (2021), accessed: 2026-02-20
10. Radford, A., Kim, J.W., Hallacy, C., Ramesh, A., Goh, G., Agarwal, S., Sastry, G., Askell, A., Mishkin, P., Clark, J., et al.: Learning transferable visual models from natural language supervision. In: *International conference on machine learning*. pp. 8748–8763. PmLR (2021)
11. Titouan, V., Courty, N., Tavenard, R., Flamary, R.: Optimal transport for structured data with application on graphs. In: *International Conference on Machine Learning*. pp. 6275–6284. PMLR (2019)

12. Yao, H., Zhang, R., Xu, C.: Visual-language prompt tuning with knowledge-guided context optimization. In: Proceedings of the IEEE/CVF conference on computer vision and pattern recognition. pp. 6757–6767 (2023)
13. Yoon, J.S., Oh, K., Shin, Y., Mazurowski, M.A., Suk, H.I.: Domain generalization for medical image analysis: A review. Proceedings of the IEEE (2024)
14. Zhang, K., Liu, X., Shen, J., Li, Z., Sang, Y., Wu, X., Zha, Y., Liang, W., Wang, C., Wang, K., et al.: Clinically applicable ai system for accurate diagnosis, quantitative measurements, and prognosis of covid-19 pneumonia using computed tomography. Cell **181**(6), 1423–1433 (2020)
15. Zhang, S., Xu, Y., Usuyama, N., Xu, H., Bagga, J., Tinn, R., Preston, S., Rao, R., Wei, M., Valluri, N., et al.: Biomedclip: a multimodal biomedical foundation model pretrained from fifteen million scientific image-text pairs. arXiv preprint arXiv:2303.00915 (2023)
16. Zhou, K., Yang, J., Loy, C.C., Liu, Z.: Conditional prompt learning for vision-language models. In: Proceedings of the IEEE/CVF conference on computer vision and pattern recognition. pp. 16816–16825 (2022)
17. Zhou, K., Yang, J., Loy, C.C., Liu, Z.: Learning to prompt for vision-language models. International Journal of Computer Vision **130**(9), 2337–2348 (2022)